EXTRAPOLATION ALGORITHMS AND OVERLOAD EFFECTS IN HIGH CYCLE FATIGUE

A Thesis

Presented to the Faculty of the Graduate School

of Cornell University

in Partial Fulfillment of the Requirements for the Degree of

Master of Science

by

Venkat Ramanan Krishnan

May 2008

ABSTRACT

The cohesive fatigue model of Ural and Papoulia [18, 19] is modified and implemented within the finite element code Abaqus. The model follows a bi-linear damage-dependent traction-displacement relation coupled with a damage evolution equation characterized by three material parameters corresponding to damage accumulation, crack closure and stress threshold.

High cycle fatigue is computationally intractable with cycle-by-cycle calculations. To make high cycle fatigue simulations possible, different extrapolation schemes have been proposed in the literature, with varying degrees of complexity, to account for the nonlinearity of the equations. Based on simple observations, two such schemes are proposed and tested in this work. A logarithmic scheme is found easy to implement, as well as capable of extrapolating the accumulation of material damage due non-constant amplitude fatigue loads. Finite element results are compared with high cycle fatigue test results for an aluminum alloy. Close matches between the test data and finite element simulations are obtained for different loading conditions.

The cohesive model is also used to capture the effect of a single peak overload, viz. crack retardation, in a ductile 316L steel alloy under plane stress conditions. The results indicate that a higher peak load results in higher fatigue crack retardation. The results also agree with experiments that suggest that strain hardening, not crack closure, is the leading mechanism for the overload effect.

BIOGRAPHICAL SKETCH

Venkat Ramanan Krishnan was born in the sleepy south Indian city of Hyderabad. After graduating from high school, he took up the Math and Sciences stream in Little Flower Junior College, Hyderabad, which helped him gain admission into I.I.T Bombay for a B-Tech in Civil Engineering. After four wonderful years in I.I.T, he decided to continue with further studies in the area of structural engineering. He was accepted with a research assistantship at the department of Civil engineering at Cornell University. He is now pursuing his PhD in Theoretical and Applied Mechanics and hopes to add a more detailed biographical sketch in his PhD dissertation.

To my dearest Parents Jayalakshmi Krishnan and Navaneetha Krishnan Govindan

ACKNOWLEDGEMENTS

I would like to thank Prof. Katerina Papoulia for providing me with the opportunity to work in this exciting project and for her constant support and encouragement without which I wouldn't have compiled this work. I would like to thank Ani Ural, now Assistant Professor at Villanova Uuniversity, for her help in getting me started with my simulations and for always patiently answering my questions through email. This work is partly a continuation of her PhD dissertation work.

Special thanks to Prof. Herbert Hui who has always been there to answer any questions/problems I've had with my research. I would also like to thank the Cornell Theory Center which facilitated the use of Abaqus on my personal computer.

I am also really glad to have found a great roommate and friend in Vijayanand Muralidharan for my first three years at Cornell. Life in Ithaca wouldn't have been half as fun without him around.

This work was supported by Task WBS 4.0 of the NASA funded Constellation University Institutes Project (CUIP) on Reusable Launch Vehicles.

TABLE OF CONTENTS

LIST OF TABLES

LIST OF FIGURES

Chapter 1

Introduction

The fatigue life of a structure is influenced by mechanical, microstructural and environmental factors and the fatigue process takes place in several different stages: nucleation, propagation, and failure. Nucleation of permanent damage occurs as a result of nanostructural and microstructural changes. This is followed by the accumulation of permanent damage and creation of microscopic cracks, called Stage I fatigue crack growth and is usually dominated by shear. Transformation of a Stage I fatigue crack to Stage II, which is the focus of this thesis, is underlined by the coalescence of microscopic flaws to form a dominant crack. During crack growth in Stage II, the propagation of the dominant crack is stable. The final stage of fatigue crack growth might be the complete failure of the structure. Fatigue life of structures is determined using total life or damage tolerant approaches. The total life approach predicts the fatigue life of a specimen as the total initiation and propagation time until failure, whereas damage tolerant design assumes that structures have inherent imperfections and flaws. For mechanical type loads, fatigue life is then calculated as the number of loading cycles needed to grow the crack to a predetermined critical dimension.

1.1 Fatigue life prediction

Various attempts have been made to fit the typical curve shown in Fig. 1.1, which is characteristic of metals. The curve relates the rate of crack growth da/dN to the stress intensity range ΔK, characteristic of a constant magnitude cyclic applied load and of the specimen geometry [3]. It exhibits a threshold stress intensity factor range, ΔK_{th},

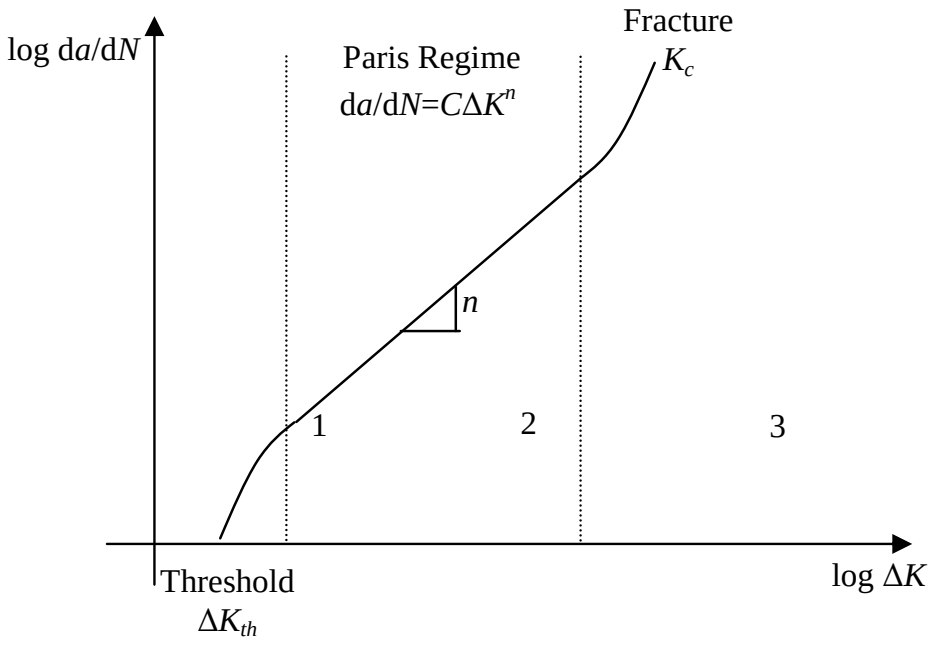

Figure 1.1: Typical fatigue crack growth behavior in metals. (Adapted from [16, 19])

below which there is no crack growth. Once this threshold value is reached, the crack starts growing at a slow rate. At intermediate values of ΔK (region 2 in the figure), crack growth shows a linear trend on a log-log scale. The final regime of fatigue crack growth, region 3, is marked by an accelerating crack growth rate and results in fracture of the specimen.

Until recently, fatigue life predictions have been based on empirical approaches. The earliest relationship developed is the Paris model [12, 13], which reproduces the linear portion of the crack growth rate plot as follows,

$$\frac{da}{dN} = C(\Delta K)^n, \tag{1.1}$$

where a is the crack length and N is the number of loading cycles. The constants C and n that appear in equation (1.1) depend not only on the material, but also on R, the ratio of minimum to maximum load, on the frequency of loading, environmental conditions,

etc. For various metals, experimental observations show that n ranges between 2 and 7.

The Paris model and similar approaches are valid under the ideal conditions of LEFM (Linear Elastic Fracture Mechanics), small-scale yielding, constant amplitude cyclic loading and long cracks. When these stringent conditions are not met, these approaches lose their predictive capability. In particular, they are unable to model the phenomenon of crack closure, i.e., the premature contact of crack faces during the unloading portion of a fatigue cycle when far-field tensile loads are still present. Fatigue crack closure is mostly observed in applications with low R values and stress intensity range close to the fatigue threshold. Elber [5] proposed that crack closure results in reducing the effective stress intensity range and therefore decreases the fatigue crack growth rate. Also, the Paris model is not useful if the load is not purely cyclic or is of variable amplitude.

1.2 Cohesive models for fatigue crack growth

Our objective is to develop a cohesive model and numerical algorithms capable of modeling fatigue crack growth in a structural component as an alternative to empirical approaches such as the Paris model. The aim is to apply the understanding of physical processes of crack formation and growth to develop a predictive method that can be used to solve engineering problems. We emphasize high cycle fatigue applications and use a modification of the traction-separation (cohesive) model proposed in [17]. The proposed model behaves as a bilinear cohesive model under monotonic loading and shows a degrading peak traction and stiffness behavior under cyclic loading due to an evolving damage parameter. This type of model can be especially useful in simulating fatigue behavior of materials which violate small scale yielding assumptions at the crack

tip. An additional advantage of using a cohesive model is that it eliminates the need for employing a crack propagation trajectory theory, since the direction of crack growth is an outcome of the calculations. Numerical implementation of this fact is an involved issue ([11] and references therein) not addressed in this thesis, since the crack path in the examples considered is predetermined (known).

The use of the cohesive zone approach in fracture problems has become common in recent years. Cohesive elements can model the nonlinear behavior occurring in the process zone ahead of the crack tip that LEFM cannot capture. Cohesive models implemented as interface elements have also been applied to fatigue problems. De Andres et al. [4] proposed a bilinear traction-displacement relationship with unloading to the origin with no cyclic degradation of the stiffness and peak traction. It was later found that, this type of model, plastic shakedown arrests crack growth after a few cycles [9]. Hence, a distinction between loading and unloading paths, allowing for hysteresis, is necessary for subcritical crack growth. Nguyen et al. [9] introduced a cohesive relationship, which, under monotonic loading is based on the potential of Xu and Needleman [20]. Roe and Siegmund [14] developed a cohesive model with unloading-reloading hysteresis obtained from the evolution of a damage variable. Increase of the damage variable resulted in decrease of the stiffness and peak load, within a bi-linear cohesive envelope. Maiti and Geubelle [8] proposed a billinear cohesive model for modeling fatigue cracks in polymeric materials. An evolution equation was introduced relating cohesive stiffness to rate of opening displacement and number of loading cycles since onset of failure. None of the models above examine the effect of R ratio, the ratio of the minimum divided by the maximum value of a cyclic load. This effect is particularly significant for models such as the one in [8], which introduces healing, since healing is known to depend on the R value.

As in [14], the proposed model introduces a damage variable, governed by an evolution equation, which accounts, in a phenomenological way, for the nonlinear processes associated with fatigue failure. The traction-displacement envelope is bilinear. Special emphasis is placed on the ability of the cohesive model to capture material healing and crack closure effects. Crack healing is known to depend on R, which is a characteristic of the loading. One aim of the model is to capture this dependence in a rational way, i.e., the model itself should not be a function of load characteristics. Unlike many phenomenological models, the proposed model contains three physically motivated parameters governing damage accumulation, crack closure and stress threshold.

The proposed cohesive model has been implemented in Abaqus standard, *V*6.5, with the help of a user subroutine (UEL), and the results compared with fatigue test results for an aluminum alloy. Close match between the test data and finite element simulations was obtained by using a single set of model parameters for different loading conditions. Two extrapolation schemes are presented to make high cycle fatigue life prediction feasible. The model is also used to predict crack retardation in a ductile steel alloy, following the application of a single peak load during constant amplitude load cycles known as the "overload effect".

1.3 Overview

The thesis is organized as follows. Chapter 2 presents the details of the cohesive model including an analysis of mathematical well-posedness as well as a brief explanation of the finite element implementation, particular aspects of which are to be found in the Appendix. Chapter 3 presents extrapolation schemes for predicting high cycle fatigue life when cycle-by-cycle simulation is not computationally feasible. Chapter 4 presents

results of laboratory experiments, and the Finite element simulations. The predictive capability of the proposed model is shown through 2D FEM simulations of cyclic fatigue tests on brittle A356-T6 compact-tension (CT) specimens under plane strain conditions. In Chapter 5, we model the well known overload effect on a ductile 316 steel CT specimen under plane stress conditions and show that the model is able to capture the crack retardation resulting from overload. Finally Chapter 6 presents a summary and conclusions.

Chapter 2

A damage-based cohesive model

The key feature of the cohesive model presented here is its use of a damage variable that controls the stiffness and peak traction. The model details are provided in the first section, and some mathematical analysis of well-posedness of the model, in the section that follows. Finite element implementation in an implicit code is briefly described in Section 2.3.

2.1 Description of the cohesive model

The proposed cohesive model exhibits a linear traction-displacement relation of the form shown in equation (2.1), in which κ is the damage variable, T and δ are the scalar effective cohesive traction and effective opening displacement, respectively (see Section 2.3), and $F(\kappa)$ is a damage-dependent elastic coefficient. The dependence of F on κ is specified by (2.2), in which δ_c is the critical opening displacement, i.e., the relative displcement at which the crack initiates and damage starts to accumulate, δ_u is the failure displacement, i.e., the crack opening displacement at which the traction becomes zero, and σ_c is the initial peak traction of the interface. The traction T is also required to satisfy the inequality $T \leq C(\kappa)$, where $C(\kappa)$ is specified by (2.3).

$$T = F(\kappa)\delta, \tag{2.1}$$

$$F(\kappa) = \frac{\sigma_c(1-\kappa)}{\kappa(\delta_u - \delta_c) + \delta_c}, \tag{2.2}$$

$$C(\kappa) = \sigma_c(1-\kappa). \tag{2.3}$$

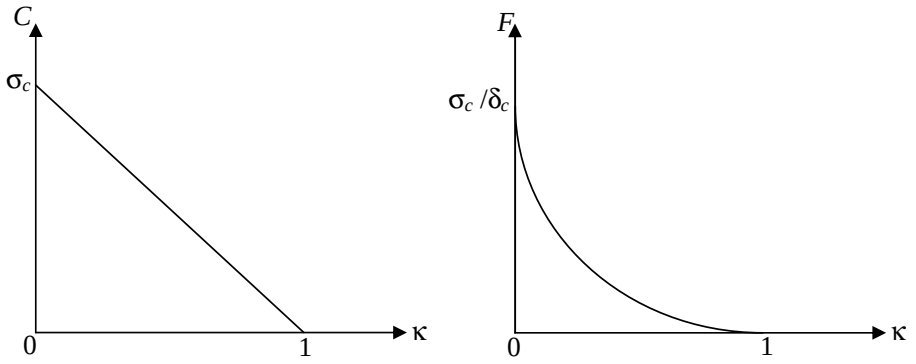

Figure 2.1: Evolution of a) peak traction, and b) stiffness with the accumulation of damage. (Reprinted from [19])

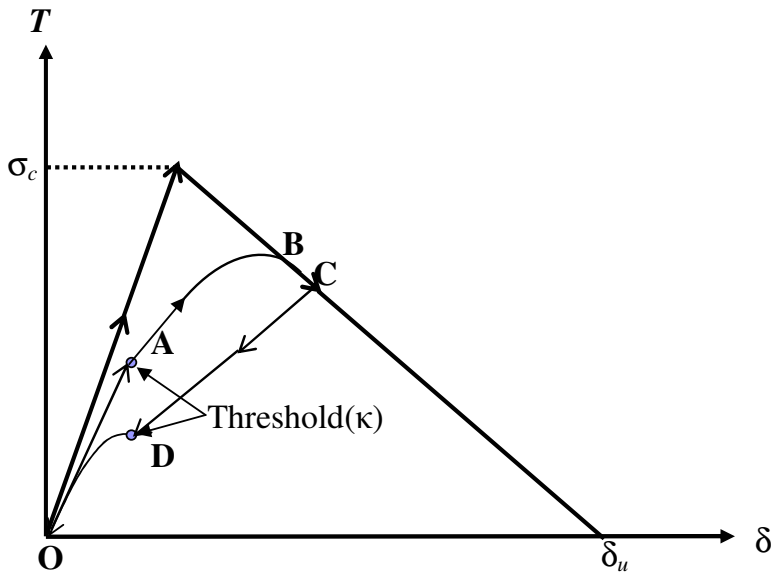

Figure 2.2: A schematic representation of the proposed cohesive traction-displacement relationship. No damage occurs during OA; damage starts increasing after the threshold at A; BC shows the descending part of the loading curve; No healing takes place during the unloading path CD; healing occurs during unloading from D to O. (Adapted from [19])

We obtain the expression for $F(\kappa)$ by first assuming $C(\kappa)$ in the form (2.3) and then requiring a bilinear traction-displacement relationship, as explained at the end of this section. Under cyclic loading the model exhibits a degrading peak traction $C(\kappa)$, and a degrading stiffness $F(\kappa)$with increasing value of κ (Fig. 2.1), resulting in eventual loss of the load transmitting ability of the material. The variable κ takes values between 0 and 1, corresponding to no damage and complete fracture, respectively. When κ equals zero, the traction T equals the peak traction, σ_c, and the opening displacement, δ, equals the critical displacement, δ_c; further, T equals zero when κ equals one. Fig. 2.2 shows a schematic representation of the proposed cohesive traction-displacement relationship. In this figure, branch *OB* is the ascending part of the loading curve, *BC* is the descending part of the loading curve, and *CO* is the unloading curve.

The evolution of the damage variable is given by:

$$\dot{\kappa} = \begin{cases} \alpha^* \kappa (T - \beta C)(\dot{\delta}) & \text{if } (T - \beta C)(\dot{\delta}) > 0, \\ 0 & \text{if } (T - \beta C)(\dot{\delta}) < 0, \\ \dot{\lambda} & \text{if } T = C \text{ and } \dot{\delta} > 0\ , \end{cases} \tag{2.4}$$

where $\dot{\lambda}$ is a free variable, α^* is a parameter that captures the rate of damage evolution, and β is a parameter that represents the threshold for initiation of damage. The parameter α^* takes on one of two distinct values for the cases of loading and unloading ($\dot{\delta} > 0$ or $\dot{\delta} < 0$) denoted by the parameters α and $-\gamma$, respectively, which as well as β are regarded as material parameters.

Equation 2.4 allows damage accretion or healing to occur only when the traction is greater or lesser than the threshold limit during loading and unloading, respectively. Physically, this can be thought of as damage accretion or healing occurring only when the work done by an effective traction (the traction on the crack surface above the thresh-

old) is positive. During loading, if the value of the traction T reaches the peak traction $C(\kappa)$, the traction is constrained to move along the envelope, $T = C(\kappa)$. This in turn forces the relationship $C(\kappa) = F(\kappa)\delta$ to hold, which defines the evolution of κ. Therefore, in this case, the third of (2.4) does not constrain $\dot{\kappa}$ at all, since $\dot{\lambda}$ is free. This is analogous to classical plasticity, in which a parameter $\dot{\lambda}$ is chosen to ensure that the stress remains on the yield surface during loading. The analogy to plasticity is not complete, however, because our model does not involve an additive strain (or opening displacement) decomposition into elastic and plastic parts.

Accordingly, when the traction-displacement relationship is tracing the descending branch of the monotonic cohesive curve, the evolution of κ is governed by the plasticity parameter, λ, and it is only a function of the current opening displacement. However, during reloading, damage depends on the rate of deformation, previous damage accumulation, cohesive traction and fatigue threshold. During unloading, the value of κ can decrease if the traction is lower than the threshold. Decreasing the damage variable during unloading is a vehicle to capture the retardation effects of crack closure.

It should be noted that the ascending and descending linear branches of the monotonic response are not explicitly defined by, but rather are a consequence of, the above equations. On the ascending branch, the relationship $T = F(\kappa)\delta$ holds with $\kappa = 0$ and hence $F(\kappa)$ is a fixed constant. Therefore, the relation between T and δ is linear on the ascending branch. When the critical traction σ_c is attained, the inequality $T \leq C(\kappa)$ becomes binding, and κ evolves according to the third of (2.4), so that $F(\kappa)\delta = C(\kappa)$ holds. The solution to this equation is a descending linear relation between T and δ.

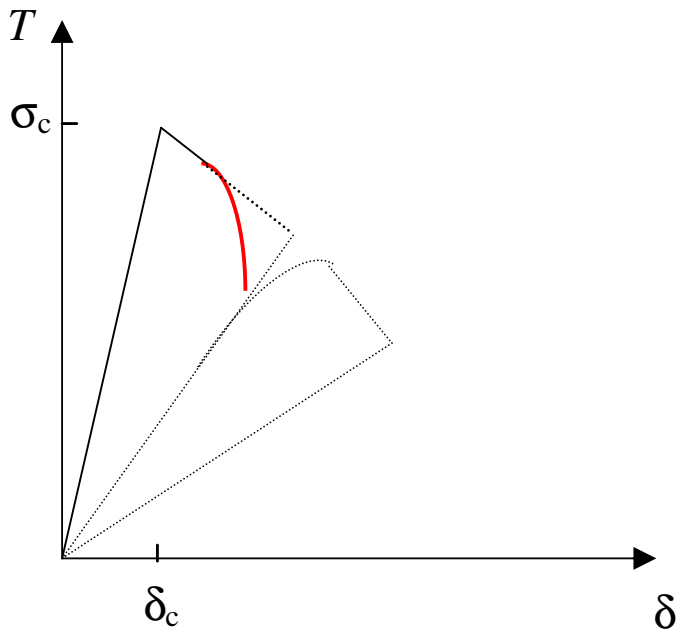

Figure 2.3: If α is too large, a trajectory from a point close to the loading envelope could diverge away from the envelope, which indicates an instability in the model. Parameter α should be small enough so that the trajectory from this point meets the loading envelope.

2.2 Well-posedness conditions on the parameter values

The model has some obvious restrictions on the parameter values such as $\alpha \geq 0$, $0 < \beta < 1$ and $\gamma \geq 0$. In this section, we will derive two subtler conditions that are necessary for the mathematical well-posedness of the model.

The first condition concerns the case that the current state of the interface is very close to, but not exactly on, the descending linear branch. In this case, for the model to be well-posed, the interface should evolve so that the state tends toward the descending linear branch. If it tends away from the branch, this creates an ill-behaved model since it implies that a small perturbation to the state can cause a large deviation in the subsequent trajectory (Fig. 2.3). A similar analysis is performed in [19].

First, consider a point on the descending branch of the model. Such a point satisfies

$F(\kappa)\delta = C(\kappa)$, and thus $\delta = \kappa(\delta_u - \delta_c) + \delta_c$. The slope $dT/d\delta$ in this case is seen to be $-\sigma_c/(\delta_u - \delta_c)$ (independent of κ and δ). Next, consider a point satisfying $\delta = \kappa(\delta_u - \delta_c) + \delta_c - \epsilon$, where $\epsilon > 0$ is extremely small. In this case, $T = F(\kappa)\delta < C(\kappa)$ so the point is below the descending branch, but only slightly. The condition for well-posedness in this case is that $dT/d\delta \geq -\sigma_c/(\delta_u - \delta_c)$, i.e., the slope of the trajectory from this point should not be less than the slope of a nearby point on the descending branch. For a point not on the descending branch, when loading is applied, i.e., $\dot{\delta} > 0$, we have

$$\frac{dT}{d\delta} = \frac{d(F(\kappa)\delta)}{d\delta} \tag{2.5}$$

$$= F'(\kappa)\frac{d\kappa}{d\delta}\delta + F(\kappa) \tag{2.6}$$

$$= F'(\kappa)\alpha\kappa(T - \beta C)\delta + F(\kappa), \tag{2.7}$$

Note that, in the case $\dot{\delta} > 0$, we used the first of 2.4, to obtain $d\kappa/d\delta$. By using the relationship $\delta = \kappa(\delta_u - \delta_c) + \delta_c - \epsilon$ and eventually dropping the ϵ, simplifying and rearranging, one obtains the following inequality:

$$\alpha \leq \frac{1}{\sigma_c\kappa(1-\kappa)(1-\beta)(\delta_u - \delta_c)}. \tag{2.8}$$

This inequality must hold for all values of κ. The denominator is maximized when

$$\kappa = 1/2 \tag{2.9}$$

so a sufficient condition that implies the above inequality is simply

$$\alpha < 4/(\sigma_c(\delta_u - \delta_c)(1-\beta)). \tag{2.10}$$

The second well-posedness condition concerns the healing part of the curve. If the healing effect is too strong, then the material may exhibit a descending branch during healing, i.e., a negative value of $dT/d\delta$, which seems unphysical and is likely to increase numerical problems. We have

$$\begin{aligned} \frac{dT}{d\delta} &= \frac{d(F(\kappa)\delta)}{d\delta} && (2.11)\\ &= F'(\kappa)\frac{d\kappa}{d\delta}\delta + F(\kappa) && (2.12)\\ &= F'(\kappa)\gamma\kappa(\beta C - T)\delta + F(\kappa), && (2.13) \end{aligned}$$

Substituting the above formula into the condition $dT/d\delta \geq 0$, simplifying and rearranging, yields the condition

$$\gamma \leq \frac{1}{\frac{\sigma_c\delta_u\kappa}{\kappa(\delta_u-\delta_c)+\delta_c}\left(\beta - \frac{\delta}{\kappa(\delta_u-\delta_c)+\delta_c}\right)\delta}. \tag{2.14}$$

This must hold for all κ, δ such that $T \leq \beta C$. Treating δ as a free variable, the denominator of the above formula is maximized when

$$\delta = \beta(\kappa(\delta_u - \delta_c) + \delta_c)/2. \tag{2.15}$$

Substitute this into (2.14) to obtain the following inequality, which is sufficient to imply (2.14):

$$\gamma \leq \frac{4}{\sigma_c\delta_u\kappa\beta^2}. \tag{2.16}$$

The worst case is when $\kappa = 1$, and thus the sufficient condition for the second well-posedness criterion is that $\gamma \leq 4/(\sigma_c\delta_u\beta^2)$.

2.3 Finite element implementation of cohesive models

The cohesive model described above governs interface elements in a finite element mesh. Our cohesive implementation, based in part on work by Ortiz and Pandolfi [10], depends on an effective scalar parameter, δ, defined as

$$\delta = \sqrt{\eta^2 \boldsymbol{\delta}_s . \boldsymbol{\delta}_s + \delta_n^2}, \tag{2.17}$$

where η is a non-dimensional coupling factor, $\boldsymbol{\delta}_s$ is the shear component, and δ_n is the normal component of the opening displacement. Our model, defines a scalar traction, T, as a function of effective displacement. This scalar traction is used in turn to define the usual vector traction through the formula:

$$\mathbf{t} = \frac{T}{\delta}(\eta^2 \boldsymbol{\delta}_s + \delta_n \mathbf{n}). \tag{2.18}$$

The finite element discretization is obtained through a virtual power equation in which the internal power consists of contributions from the bulk part of the domain and from interfacial tractions, governed by the traction-separation relationships defined in the previous section. The interface terms are discretized with duplication of element nodes on the interfaces, and the virtual power equation thus leads to a discrete set of nonlinear equations in the nodal displacements. The model was implemented within the finite element code Abaqus [2] using a user subroutine within the UEL scheme, which lets users code in their own user elements for use with the Abaqus solver. Details of the implementation of the proposed cohesive model governing the interface cohesive elements are given in the Appendix.

Chapter 3

Extrapolation Schemes for predicting high cycle fatigue life

Fatigue tests can be simulated through cycle-by-cycle computation of the change in displacements and evolution of the damage variable. However, computational times can be prohibitively long for high-cycle fatigue applications.

In the current work, the fatigue tests that are simulated run for as long as half a million cycles. One cycle in a 3GHz PC takes about 5 minutes, therefore, running cycle-by-cycle simulations is not practically feasible. To this end, an extrapolation scheme that extrapolates only the damage variable is used , whereby only a few loading cycles are analyzed explicitly, and the solution state computed from these cycles is used to predict the state at a future cycle. An example of such an extrapolation scheme may be found in [4], in which the change of damage was extrapolated linearly by a large number of cycles to predict the damage at a later stage. However, damage evolution at a Gauss point, in general, can be nonlinear, as is indeed in the model being analyzed. Use of a linear extrapolation scheme precludes the use of large extrapolation increments necessary to make the problem computationally feasible. When large increments are used with a linear scheme, convergence problems arise from instabilities introduced by rapid accumulation of damage in the process zone. In our computational experiments, small extrapolation increments, of the order of $N = 10$, are needed to avoid this, which do not give the required computational efficiency. Hence, this scheme is not suitable for our purposes.

The extrapolation scheme in [17, 19] is based on iteration of the damage variable using the implicit nonlinear equation for κ_{n+1} (see Appendix), as many times as the

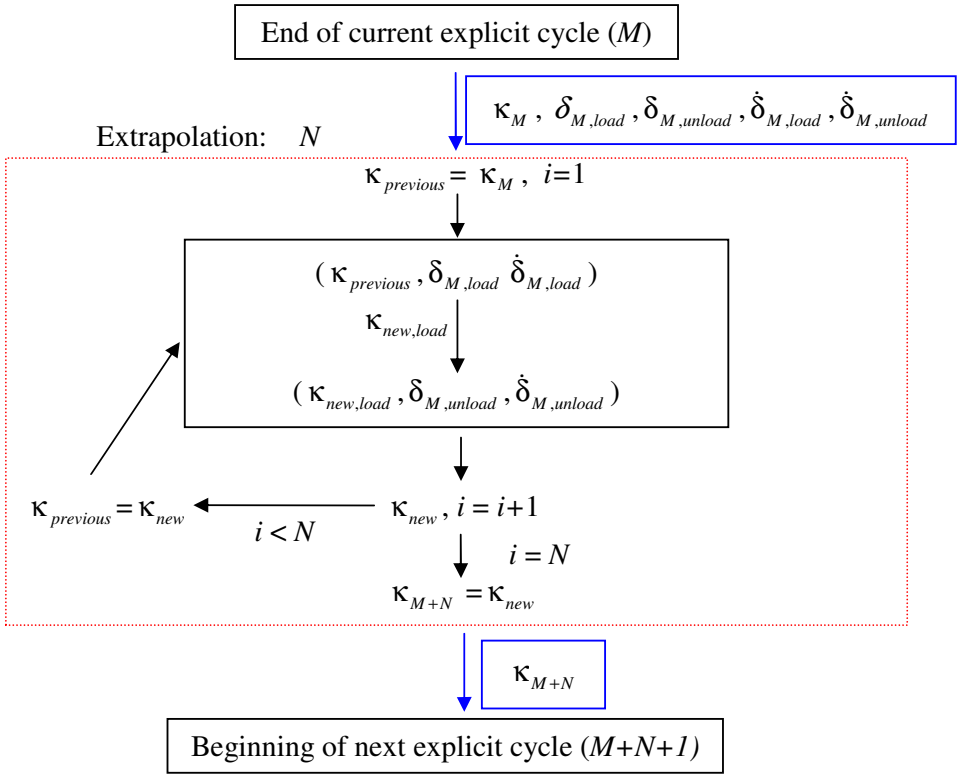

Figure 3.1: Iterative extrapolation scheme. (Reprinted from [19]).

desired number of extrapolation cycles, say N. This equation calculates the damage based on the current displacement δ_{n+1}, previous displacement δ_n and the previously accumulated damage κ_n. At the end of each cycle, a new damage value is calculated by iterating this equation N times while the displacement values for evaluating T (traction), are kept constant. At the end of N cycles a new damage value is determined and this is taken as the starting point for the next explicit cycle. N should be such that the change in the opening displacements remains small. This condition is necessary in order to be able to capture the cycle-by-cycle behavior. A flowchart of the extrapolation scheme is shown in Fig. 3.1.

This extrapolation scheme is easy to implement, but results in convergence problems when used with the cohesive model presented here. It also assumes that the effective opening displacement does not change for the extrapolated number of cycles, which is

not necessarily true.

3.1 Empirical extrapolation scheme

In this work an extrapolation scheme is developed based on the distribution of the damage variable in the process zone ahead of the crack tip. The crack length after N loading cycles is a function of N, α and other model parameters. Let a_{crit} be the critical value of crack length at which the crack growth becomes unstable. For a given value of α, let $N_{\text{crit}}(\alpha)$ be the number of cycles required for the crack length to reach a_{crit}. (For now, we suppress dependence on the other parameters of the material model and load by assuming all of these are fixed.)

It is clear that $N_{\text{crit}}(\alpha)$ will be a decreasing function of α. For large values of α, $N_{\text{crit}}(\alpha)$ can be determined via explicit cycle-by-cycle simulation. For smaller and more realistic values of α, however, an extrapolation scheme is necessary to estimate $N_{\text{crit}}(\alpha)$ and, more generally, crack length as a function of N.

Our extrapolation scheme is as follows. Let $\kappa(N, \alpha)$ denote the vector of the values of κ at all Gauss points of the model after N loading cycles when the damage accumulation parameter is α. Consider two values of this parameter, say α_1 and α_2, such that $\alpha_1 > \alpha_2$. Suppose that $N_{\text{crit}}(\alpha_1)$ is already known or is estimated, and an estimate of $N_{\text{crit}}(\alpha_2)$ is sought. Fix a number of cycles, say N_2, such that it is feasible to explicitly simulate N_2 load cycles with α_2 as the parameter, thus yielding $\kappa(N_2, \alpha_2)$. Next, determine the value of N_1 that minimizes $\|\kappa(N_1, \alpha_1) - \kappa(N_2, \alpha_2)\|$ measured in the Euclidean norm. Let $\rho(\alpha_1, \alpha_2)$ be N_2/N_1, where N_1 is the optimal value. Regard $\rho(\alpha_1, \alpha_2)$ as a scaling factor to be used as follows: crack progress over N cycles with parameter α_1 is assumed to equal crack progress after $N\rho(\alpha_1, \alpha_2)$ if α_2 were used. In particular, estimate $N_{\text{crit}}(\alpha_2) =$

$N_{\text{crit}}(\alpha_1)\rho(\alpha_1, \alpha_2)$.

The procedure described in the previous paragraph can be applied to a sequence of α's that differ from each other by factors of 2; the largest α in the sequence is chosen so that $N_{\text{crit}}(\alpha)$ is determined by explicit simulation, and the smallest is chosen so that $N_{\text{crit}}(\alpha)$ is close to experimentally determined values for high-cycle fatigue, i.e., on the order of 10^6.

Computational experiments with this extrapolation scheme are summarized in Tables 3.1–3.3. The entries in this table have the following meanings. The first row of numbers shows explicitly computed values of $N_{\text{crit}}(\alpha_{high})$, which are available only for larger values of α_{high}. The entries in the table from the second row downward are extrapolated value of $N_{\text{crit}}(\alpha_{high})$ derived from explicit cycle simulation using parameter α_{small}. The extrapolation is done using the scheme described above of matching damage values from α's that differ by factors of 2. Evidence for the validity of the extrapolation scheme is the observation that similar estimates of $N_{\text{crit}}(\alpha_{high})$ are obtained regardless of the choice of α_{small} (i.e., the entries in the table in any particular column are very close to one another).

From these computational experiments, we conclude that $N_{\text{crit}}(\alpha)$ is inversely proportional to α^*, where α^* is α in the case of $R = 0.5$ and both α and γ for $R = 0.1$, i.e., the scaling factor defined earlier satisfies the equation $\rho(\alpha_1, \alpha_2) = \alpha_1/\alpha_2$. For the $R = 0.5$ loading, the value of γ is not important since the loading does not allow for any crack healing to occur. Hence, the number of cycles to failure varies inversely as α only, for a given β. But for $R = 0.1$ loading, the number of cycles to failure varies inversely as both α and γ i.e., on scaling both α and γ by the same amount, the number of cycles to failure scales inversely. Based on this extrapolation scheme, the parameters α, β and γ were determined for the case of low cycle fatigue and then α and γ were scaled inversely

Table 3.1: Results from computational experiments testing the extrapolation scheme for parameter $\beta = 0.2$ and loading ratio $R = 0.5$. See Section 3 for a description of the entries.

	α_{high}							
	0.20	0.14	0.10	0.05	0.01	0.005	0.001	0.0005
explicit	481	698	987	-	-	-	-	-
α_{small}=0.20	-	-	-	1961	9806	19740	1.02E5	2.11E5
α_{small}=0.14	-	-	-	1976	9931	19903	1.02E5	2.09E5
α_{small}=0.10	-	-	-	1990	9960	19980	1.02E5	2.07E5
α_{small}=0.05	-	-	-	-	9990	20020	1.01E5	2.03E5
α_{small}=0.01	-	-	-	-	-	20000	1.01E5	2.01E5
α_{small}=0.005	-	-	-	-	-	-	1E5	2.015E5
α_{small}=0.001	-	-	-	-	-	-	-	2.04E5

to obtain the corresponding parameters for the high cycle fatigue case.

The empirical extrapolation scheme shown here is obviously very involved, time consuming and cannot be implemented in a finite element code. One is not sure if the same relationship between crack length and number of cycles would apply for a different loading case or a different specimen. We use this this extrapolation scheme and the same specimen and loading conditions to verify the extrapolation scheme that we develop next.

Table 3.2: Results from computational experiments testing the extrapolation scheme for parameter $\beta = 0.15$ and loading ratio $R = 0.5$.

	α_{high}								
	0.20	0.15	0.10	0.05	0.01	0.005	0.001	0.0005	0.0001
explicit	425	575	875	-	-	-	-	-	-
α_{small}=0.20	-	-	-	1936	8682	17602	9.08E4	1.88E5	-
α_{small}=0.15	-	-	-	1949	8769	17753	8.87E4	1.86E5	-
α_{small}=0.10	-	-	-	1962	8867	17828	9.01E4	1.85E5	-
α_{small}=0.05	-	-	-	-	9859	19780	99649	2.005E5	1.17E6
α_{small}=0.01	-	-	-	-	-	19718	98889	1.979E5	1.01E6
α_{small}=0.005	-	-	-	-	-	-	98689	1.975E5	1.006E6
α_{small}=0.001	-	-	-	-	-	-	-	1.974E5	1.005E6
α_{small}=0.0005	-	-	-	-	-	-	-	-	9.96E5

Table 3.3: Results analogous to Table 3.1 using parameter $\beta = 0.2$ and loading ratio $R = 0.1$.

	α_{high}					
	0.10	0.05	0.01	0.005	0.001	0.0006
explicit	500	-	-	-	-	-
α_{small}=0.01	-	1002	5041	10125	50000	83500
α_{small}=0.05	-	-	5029	10059	50094	83658
α_{small}=0.01	-	-	-	16094	50294	83823
α_{small}=0.005	-	-	-	-	50294	83823

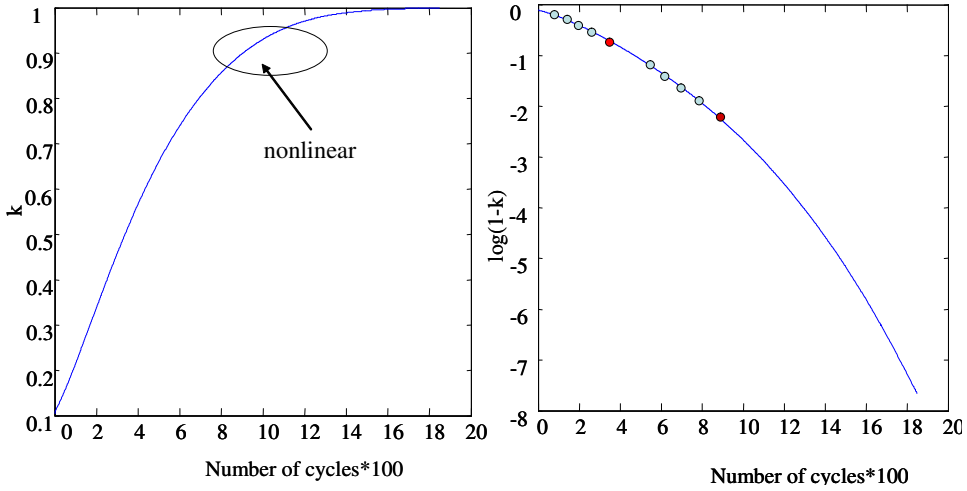

Figure 3.2: a) Evolution of damage variable κ exhibiting limiting value kappa=1, and b) Evolution of $\log(1-\kappa)$ exhibiting no limiting value

3.2 Logarithmic extrapolation

Keeping in mind that damage accumulation in the proposed model is highly nonlinear in the vicinity of its limiting value $\kappa = 1$ (Fig. 3.2), we extrapolate the value of $log(1-\kappa)$ instead, since $log(1-\kappa)$ is a smooth function of number of cycles with no limiting values. Since κ itself has a limiting value of 1, any extrapolation scheme using κ would require a limit on the number of extrapolated cycles in order to respect this constraint.

The extrapolation scheme works as follows: after five explicit fatigue cycles, the value of κ is extrapolated by N, the number of desired extrapolation cycles, using the values of κ at the previous four cycles by means of a least squares regression. We use values of κ from the previous four rather than the previous five cycles, so that the value of an extrapolated κ is not used for evaluating the next extrapolation. Note that κ from the fifth previous cycle is an extrapolated value. This allows the damage variables evaluated in the process zone undergo at least one explicit cyclic computation before proceeding with the next extrapolation process. This helps prevent numerical instabilities, which

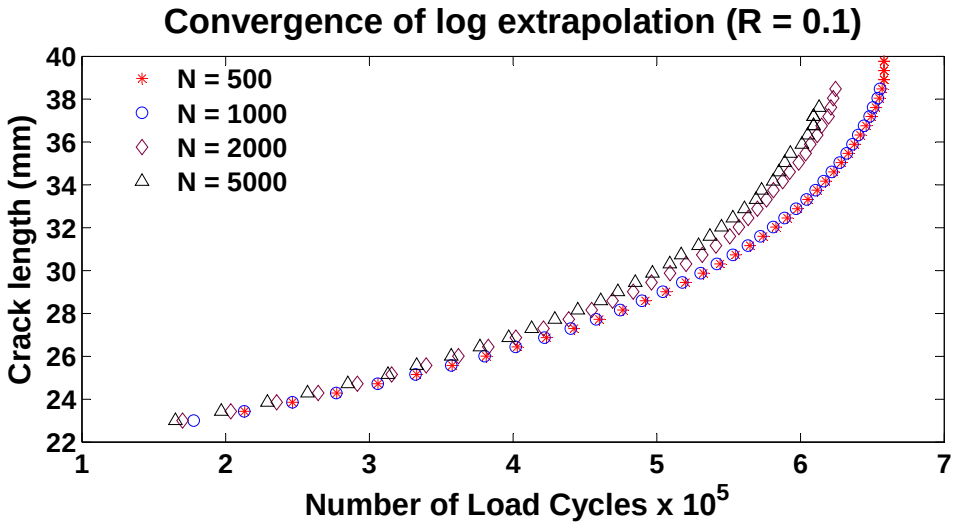

Figure 3.3: Logarithmic based extrapolation scheme for $R = 0.1$. The extrapolation becomes accurate as the size of the extrapolation increment is decreased. The curve for $N = 500$ almost lies on $N = 1000$, so $N = 1000$ is a good choice.

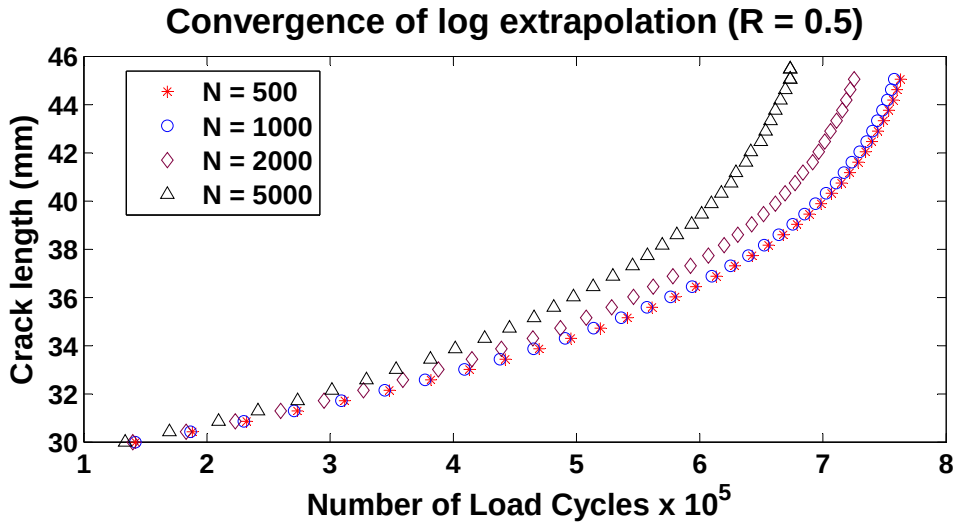

Figure 3.4: Logarithmic based extrapolation scheme for $R = 0.5$. The extrapolation becomes accurate as the size of the extrapolation increment is decreased. The curve for $N = 500$ almost lies on $N = 1000$, so $N = 1000$ is a good choice.

result in premature cracking ahead of the crack tip. Algorithmically, let κ_1, κ_2, κ_3, κ_4, and κ_5 be the values of the damage variables at a Gauss point evaluated at cycles *M*, *M+1*, *M+2*, *M+3* and *M+4*. Assuming κ_1 is a result of the previous extrapolation, then κ_2, κ_3, κ_4, and κ_5 are obtained from direct cycle-by-cycle computations starting with κ_1. Letting

$$y_i = \log(1 - \kappa_i) \tag{3.1}$$

$$x_i = M, \tag{3.2}$$

regression equation is

$$y_N = a + b * x_N \tag{3.3}$$

$$b = \frac{\Sigma x_i y_i - \frac{\Sigma x_i \Sigma y_i}{N}}{\Sigma x_i^2 - \frac{(\Sigma x_i)^2}{N}} \tag{3.4}$$

$$a = \frac{\Sigma y_i - b\Sigma x_i}{N} \tag{3.5}$$

Using the equations above, the extrapolated value of κ can be evaluated for different values of *N*. The plots of crack growth as a function of number of load cycles converges as the size of the extrapolation increment is reduced and we see that the plot for $N = 1000$ almost matches the plot for $N = 500$ as shown in Figs. 3.3 and 3.4. The computational cost associated with this approach is equivalent to the cost of extrapolating by N/5 cycles after each explicit cycle.

Chapter 4

Fatigue simulations on A356-T6 CT specimen

4.1 Finite element simulations

Fatigue tests were performed on A356-T6 cast aluminum alloy CT specimens with a thickness of 9.1 mm for R ratios equalling 0.1 and 0.5 [15] following ASTM E647 [1] under constant amplitude loading. The *R-ratio* of a pure periodic force-driven loading is defined to be the ratio of lowest load level per cycle to the highest load level [3]. Fig. 4.1 shows the specimen dimensions for the fatigue tests. The loading and initial pre-crack locations of the specimens for both R ratios are given in Table 4.1. During these tests, incremental crack growth lengths and the corresponding number of cycles were recorded. A definite R ratio effect in the test results, indicating the role of crack closure, was reported and discussed in [15]. For further details, the reader is referred to [19].

The above fatigue experiments were simulated using the proposed cohesive model. The local cohesive strength of the material σ_c, and work of separation G_c, were determined from monotonic fracture tests of A356-T6 Aluminium alloy CT specimens [19]

Table 4.1: Initial and final locations of crack in CT test specimens and magnitude of the applied fatigue loading.

Loading	P_{min}(N)	P_{max}(N)	a_0(mm)	a_f(mm)
$R = 0.1$	414.444	4144.444	23	38
$R = 0.5$	1615	3230	30	45

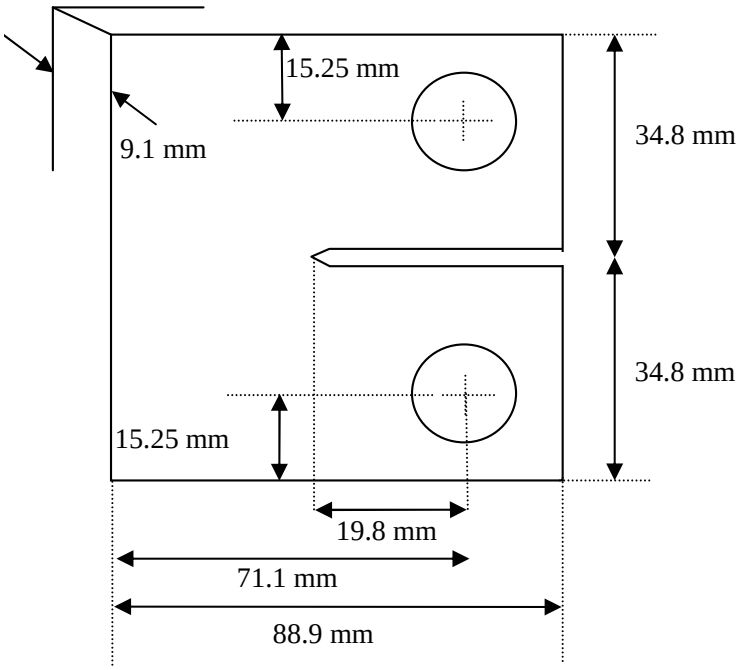

Figure 4.1: CT specimen for fatigue tests. ([15])

and found to be $\sigma_c = 190Mpa$ and $G_c = 5.5N/mm$. Similarly, material properties for the bulk were obtained in [19] from a monotonic tensile test and were found to be: $E = 70000$MPa, $\mu = 0.33$, $\sigma_y = 229$MPa. As in [19], the bulk material is assumed to be elastic-perfectly plastic.

The analyses for the Al356-T6 Aluminium alloy were performed under plane strain assumptions. The location of cohesive elements, placed in the direction of crack growth, and the fatigue starter notch in the CT specimen are marked in Fig. 4.2. The finite element mesh used was composed of 13,080 quadrilateral elements and 60 cohesive elements and is shown in the undeformed and deformed configuration in Fig. 4.2. For the $R = 0.1$ simulation, 18 time steps were used and for the $R = 0.1$ simulation, 10 time steps were used per load cycle as shown in Fig. 4.3. The number of steps per load cycle are chosen so that each load step is a 10% increment or decrement of the peak load. The

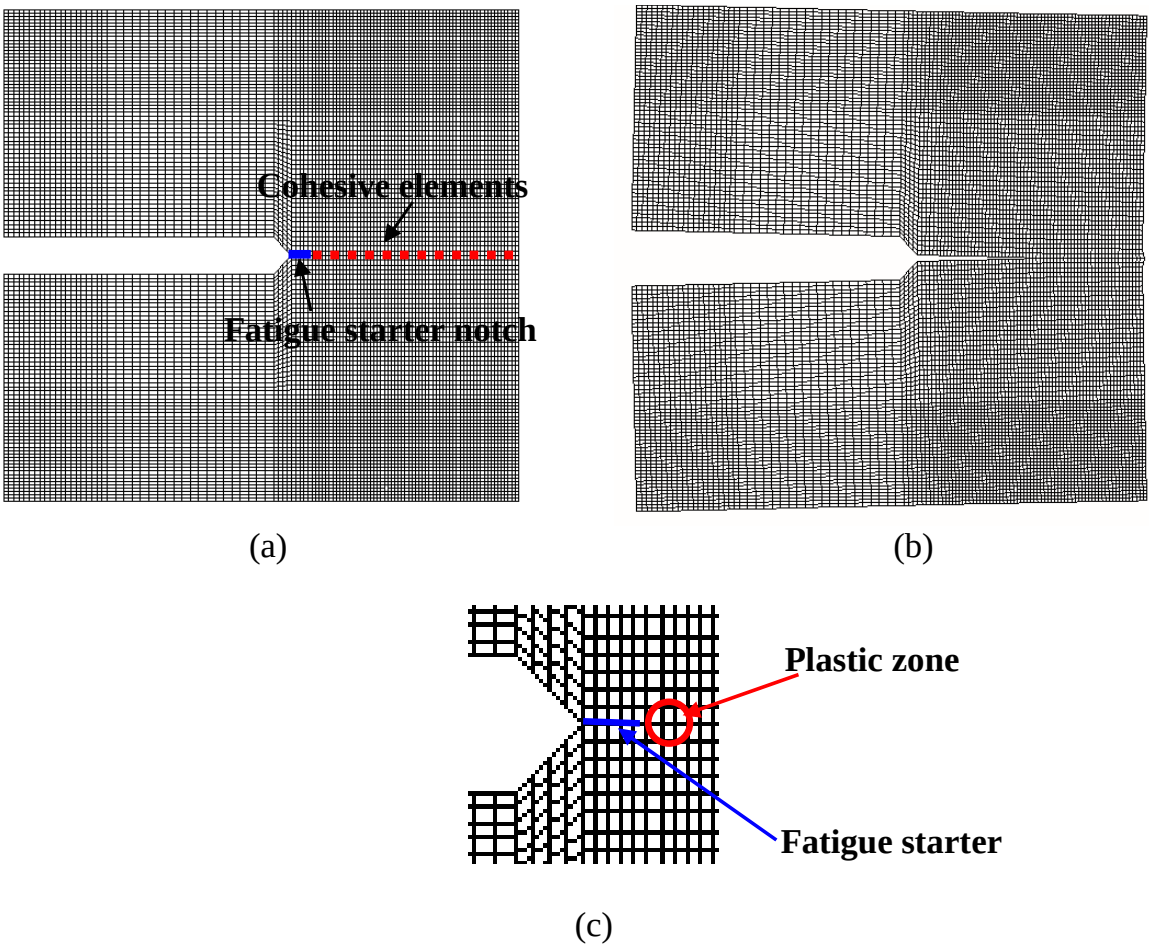

Figure 4.2: An undeformed finite element mesh of CT specimen (top left), a deformed mesh at the end of the simulations (top right), and a close-up of the notch tip region (bottom). The displacement magnification factor is 5. (Reprinted from [19])

fatigue simulations performed in this section involve determining the parameters, α, β and γ in the damage evolution equations (2.1). which define the evolution of damage. These parameters are defined as constants for the material regardless of loading conditions. The values of the parameters are chosen by trial and error such that the model is able to predict the experimental response very closely.

Under plane strain assumptions, the estimated plastic zone size can be calculated as

$$r_p = \frac{1}{3\pi}\left(\frac{K_{Ic}}{\sigma_y}\right)^2, \tag{4.1}$$

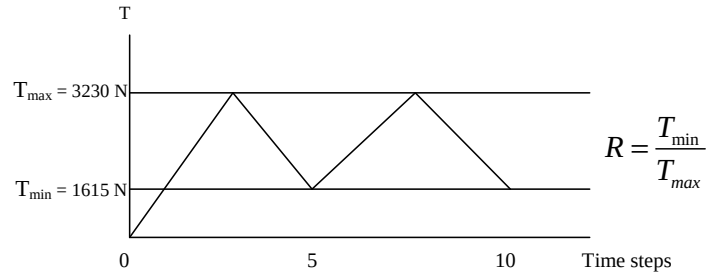

a) R = 0.5

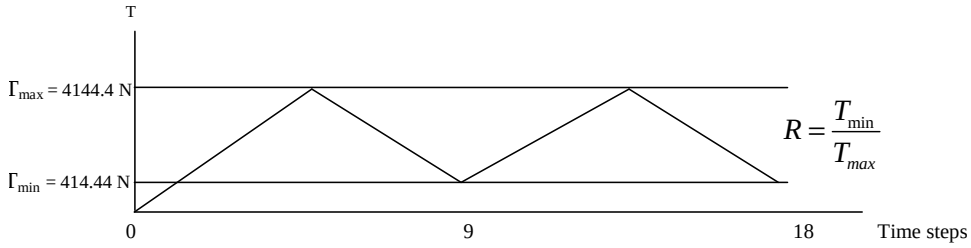

b) R = 0.1

Figure 4.3: Fatigue loading cycle for FEM simulations a) R = 0.5, b) R = 0.1

which gives a plastic zone size of 1.3 mm for a CT specimen 9.1 mm thick [3]. According to this calculation, the cohesive zone is spanned by two cohesive elements. Increasing the number of cohesive elements in the plastic zone did not affect the results. This indicates that the size of the cohesive elements was small enough to resolve the plastic zone.

Simulations of the fatigue tests were then carried out using the cohesive parameters determined from the monotonic tests and simulations. Section 4.2 presents sensitivity studies on how the fatigue life of the CT specimen is affected by the parameters α, β and γ. The results of the simulations follow along with their comparison to test data.

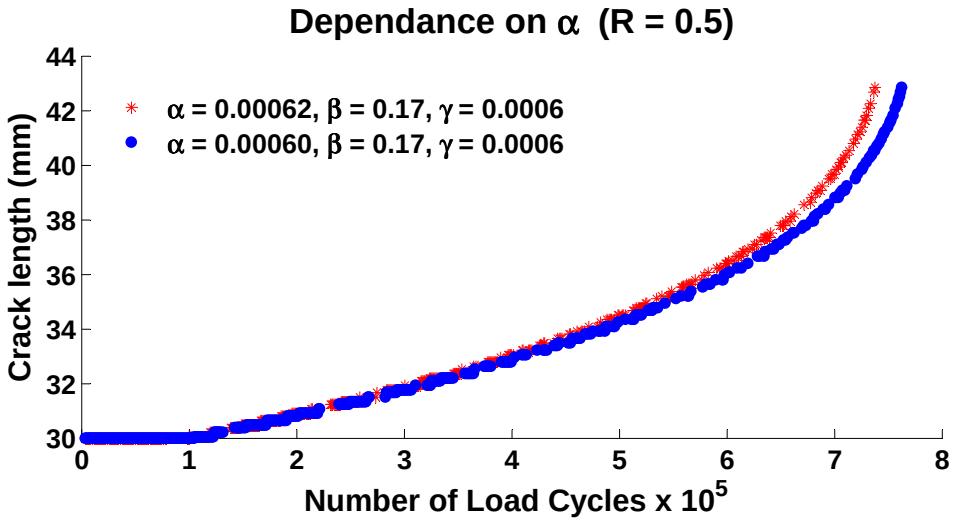

Figure 4.4: Comparison of fatigue crack growth simulation results with varying α for $R = 0.5$ loading.

4.2 Sensitivity studies and results

In this section, the sensitivity of simulation results to the damage evolution parameters, α, β and γ is investigated.

Fig. 4.4 shows the effect of changing the value of α for $R = 0.5$. As expected, increasing (decreasing) the value of α increases (decreases) the rate of damage accumulation and therefore the crack growth rate.

Fig. 4.5 shows the effect of changing the value of β for $R = 0.1$. As expected, increasing (decreasing) the value of β decreases (increases) the rate of damage accumulation and therefore the crack growth rate. A higher β indicates a higher threshold for damage accumulation, which slows down the crack propagation rate. A higher β also means that healing is more active, which further slows the crack.

Fig. 4.6 shows the effect of changing the value of γ for $R = 0.1$. As expected, increasing (decreasing) the value of γ decreases (increases) the rate of damage accu-

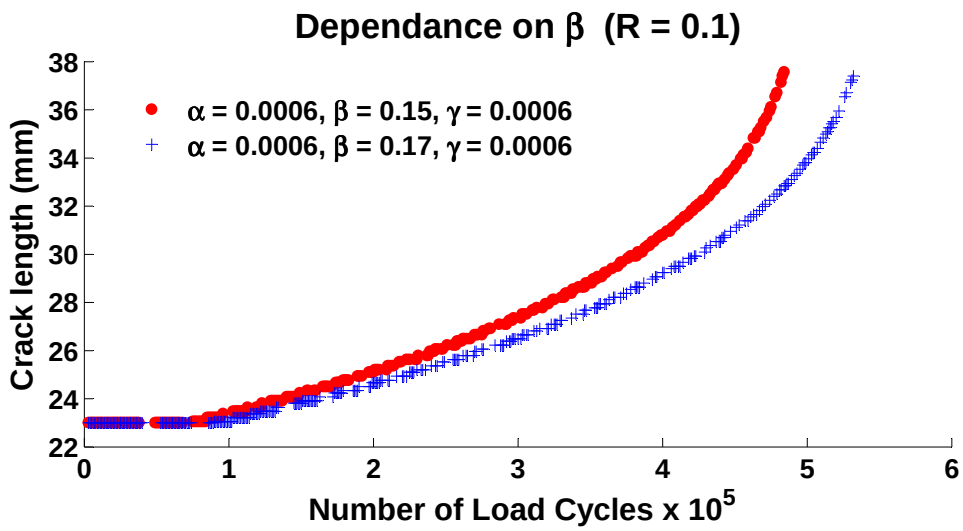

Figure 4.5: Comparison of fatigue crack growth simulations results with varying β for $R = 0.1$ loading.

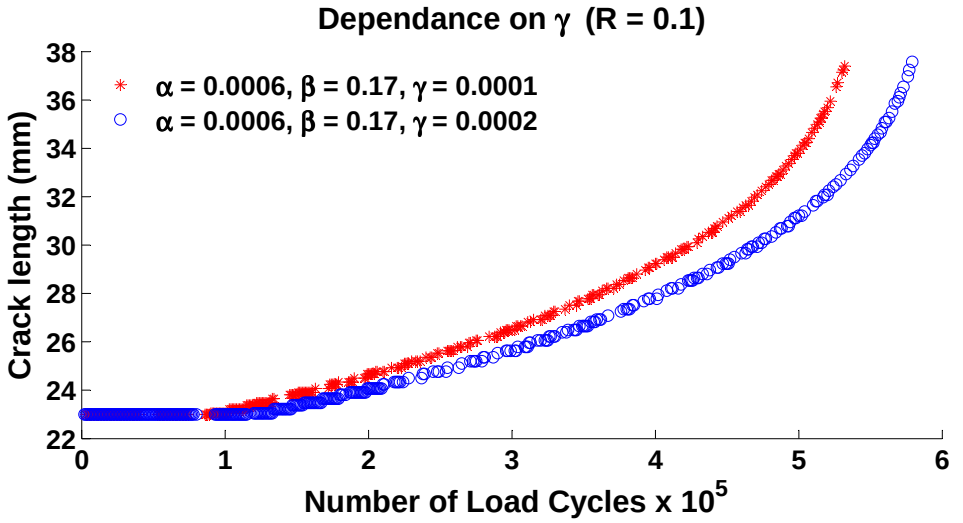

Figure 4.6: Comparison of fatigue crack growth simulation results with varying γ for $R = 0.1$ loading.

mulation and therefore the crack growth rate. A higher γ indicates a larger amount of healing during unloading which slows down the crack propagation rate.

The predictive capability of the proposed model is established through simulation of the fatigue crack growth tests described in the previous section. The results using

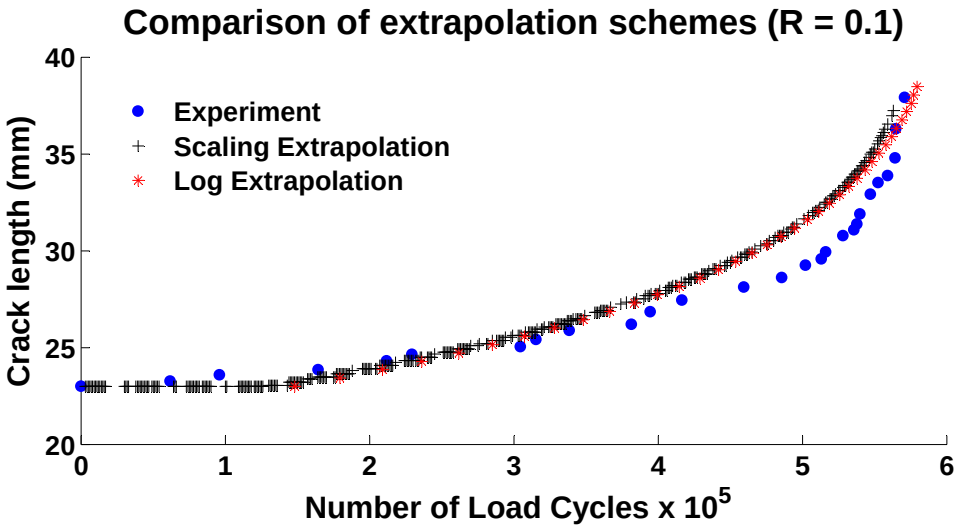

Figure 4.7: Fatigue crack growth simulation results obtained with empirical (scaling) extrapolation scheme and the log extrapolation scheme, compared with test data for loading ratio $R = 0.1$. ($\alpha = 0.00012$, $\beta = 0.14$ and $\gamma = 0.00085$).

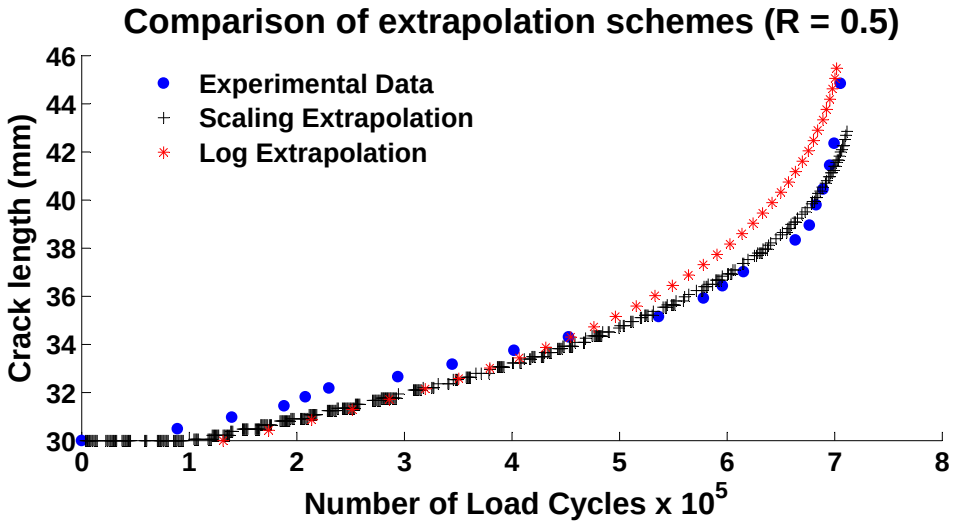

Figure 4.8: Fatigue crack growth simulation results obtained with empirical (scaling) extrapolation scheme and the log extrapolation scheme, compared with test data for loading ratio $R = 0.5$. ($\alpha = 0.00012$, $\beta = 0.14$ and $\gamma = 0.00085$).

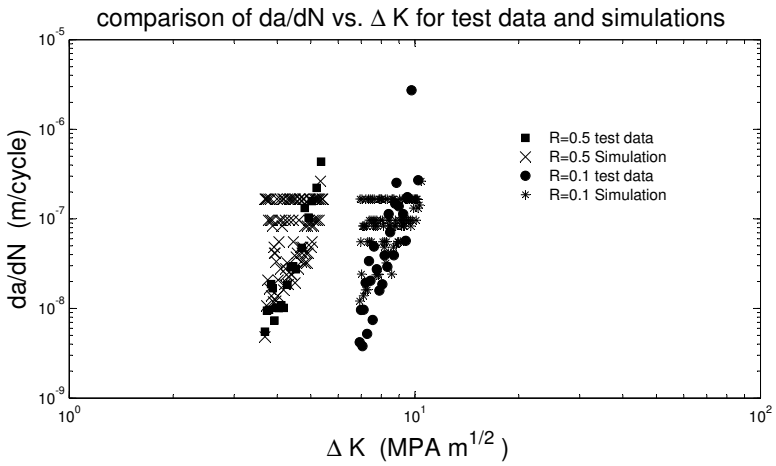

Figure 4.9: da/dN vs. K curves obtained from the test data and from FE simulations for loading ratios $R = 0.1$ and $R = 0.5$.

the logarithmic extrapolation scheme closely match the results using the empirical extrapolation scheme, whose accuracy was established earlier. Figs. 4.7 and 4.8 show simulation results for the $R = 0.1$ and $R = 0.5$ tests, respectively, using the empirical and the log extrapolation schemes for the same set of parameters $\alpha = 0.00012, \beta = 0.14$ and $\gamma = 0.00085$, and their comparison with the test data. The results especially those for $R = 0.5$, show good agreement with the fatigue crack growth test data of [15]. The results for $R = 0.1$ also show good agreement; however, the crack growth rate is not as high as in the test results at larger crack lengths, and shows a uniform increase. Since there is no explicit dependence of the model on crack length, the kink seen in the experiment is not captured in the simulations. The graphs show simulation results up to the point of unstable crack growth as observed in the tests. The instability points predicted by the simulations are very close to the experimentally observed values. Table 4.2 shows comparison of predicted initiation and failure cycles with the test data.

The results presented in this section can also be investigated in the form of crack growth rate versus stress intensity factor. The following equation [1] is used to reduce the test data and the simulation results to the information in Fig. 4.9:

Table 4.2: Initiation and failure cycles from tests and simulations for both R ratios.

Loading	Initiation Cycle	Failure cycle
Simulation $R = 0.1$	128000	563000
Test $R = 0.1$	61853	570830
Simulation $R = 0.5$	101000	709000
Test $R = 0.5$	89050	705440

$$\begin{aligned} \Delta K &= \frac{\Delta P}{BW^{1/2}} f(a/W), \qquad (4.2) \\ f(\frac{a}{W}) &= \frac{(2+\frac{a}{W})(0.886+4.64(\frac{a}{W})-13.32(\frac{a}{W})^2+14.72(\frac{a}{W})^3-5.6(\frac{a}{W})^4}{(1-\frac{a}{W})^{3/2}}, \end{aligned}$$

where a is the crack length, ΔP is the tensile load range, B is the specimen thickness and W is the specimen width. As seen in Fig. 4.9, the rate of crack growth and the ΔK values predicted by the simulations match the test data. If each data group were reduced to a straight line, the simulation and the test data would predict slightly different slopes. This difference is more noticeable in the simulation results for $R = 0.1$.

The question of existence of another triplet of parameters, which could fit the experimental data was also investigated, to check if the parameters α, β and γ are unique for a given material. A series of simulations was performed using higher values of the parameters. The observation from these simulations was that as the values were increased, crack growth first occurred at a cycle much later than observed in the tests. Furthermore, crack growth occurred at a much faster rate in order to attain the instability point at a cycle comparable to the tests. As a result, in order to match closely the initiation cycle, the instability cycle, as well as the overall behavior in between these two events, the parameters appear to be unique.

Chapter 5

Modelling overloads with cohesive elements

5.1 Overloads in 316L steel alloy

Fatigue crack growth rates are well known to be decelerated by the acting of overloads, which tend to cause an initial increase of the crack growth rate, followed by fast decrease before the final return to steady state crack propagation. The cause is usually attributed to plasticity induced crack closure, strain hardening, crack tip blunting, crack deflection, and/or branching, depending on the toughness of the material.

The empirical extrapolation scheme, as already mentioned, cannot be used to predict fatigue life of specimens subject to non-constant amplitude loading. Hence the logarithmic extrapolation scheme is very useful in predicting phenomena like the overload effect. The application of a single peak load to a fatigue crack, growing under constant amplitude loading conditions, is long known to introduce crack retardation. Wheatley *et al* [7] performed experiments on ductile 316L steel, which indicated that overall crack retardation under plane stress conditions is related to strain hardening and residual compressive stresses in the plastic region of the overload.

Our objective here is to show that the cohesive model can be used to predict crack retardation following overloads, and also captures the physics behind the mechanism. Plane stress simulations were performed on a CT specimen of width 40mm and thickness 6mm [6], with a pre-crack 12mm long, and a high cycle fatigue pre-crack of length 6mm. A loading ratio of $R = 0.1$ was applied with a minimum load of 3KN. An elastic-plastic material model with linear kinematic hardening, was used to model the bulk elements. The material properties of the specimen used in the experiments were: $E = 1.93$

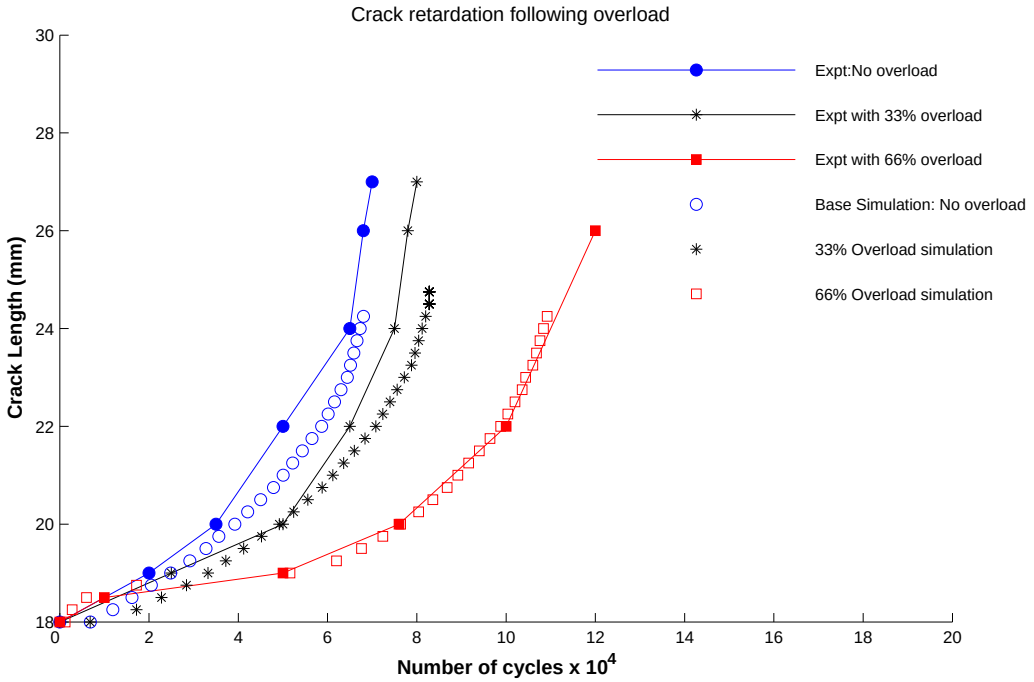

Figure 5.1: Illustration of overload effect : Crack retardation following application of a single peak overload increases with increasing value of the peak load

GPa, $\mu = .33$,$\sigma_u = 588$MPa, $\sigma_y = 334$KPa.

Fig. 5.1 shows the simulation results for single peak overloads. Crack retardation is more pronounced when the overload is higher. The crack accelerates immediately following the overload, but slows down within a few cycles, and then goes to a minimum before eventually reaching the pre-load crack growth rate. The simulations are able to closely predict the experimental results. It was observed that using the extrapolation scheme soon after the application of the overload, caused the FE program to crash, due to the sudden increase in the value of the damage variables in the process zone. Hence, no extrapolation is performed for a few cycles following the overload application, so that the overload effect is captured in explicit cycles. Of course, the damage extrapolation scheme is used to simulate the part of the experiment in which the increased load

amplitude is held constant for many cycles, i.e., after the application of overload.

Wheatley *et al* in [6, 7],explain the overload effect based on field emission scanning electron microscopy (FASEM) observations, which suggest that strain hardening and residual stresses, caused by the plastic deformation due to the peak overload are responsible for crack retardation. They hypothesize a small fatigue damage zone ahead of the crack tip to explain the immediate acceleration and subsequent retardation in crack growth. They argue that crack closure is not a significant cause of the overload effect. Our FEM simulations corroborate their experimental results. Indeed setting γ, the crack closure parameter, equal to zero in the cohesive model, made little difference in the crack retardation plots. The physical interpretation is as follows: due to the sudden increase in load, beyond the yield limit of the highly ductile material, strain hardening plasticity produces residual stresses in the plastic region, which envelopes the damage zone. These force the fatigue damage to be minimal and slow down the fatigue crack. Hence, even though the crack accelerates immediately following application of the peak load, due to a high value of K_{II}, the subsequent size of the damage zone ahead of the crack tip is reduced. The crack growth rate thereafter slowly increases, as the size of the damage zone ahead of the crack tip increases to its pre-load value. In accordance to the theory presented in [6, 7], change in the yield stress of the material made a significant difference in the fatigue crack growth. As the yield stress was reduced towards that of a more brittle material, crack retardation was reduced to a point that it completely disappeared after the initial transient acceleration.

Chapter 6

Summary

A damage-based cohesive model and algorithmic scheme for its finite element implementation is developed for simulating fatigue under cyclic loading. The model introduces three material parameters in defining the rate of evolution of a damage variable, κ, which leads to eventual crack growth. The three parameters have simple physical interpretations: they determine the rate of damage accumulation, a threshold value for accumulation of damage and a rate of healing representing crack closure effects.

The cohesive model is tested on a relatively brittle aluminum alloy CT specimen, and the results of the finite element simulations compare favorably with the experimental results. A single set of parameters is determined that fits two tests under different loading conditions. A sensitivity study of the parameters affecting the simulation results is carried out. This allows for the calibration of the model for a specific material and use of this set of parameters under different loading conditions.

In order to simulate high cycle fatigue crack growth in both brittle and ductile materials, a logarithmic damage extrapolation scheme is developed for use with a cohesive zone model exhibiting nonlinear damage evolution. The algorithmic scheme for the finite element implementation of the cohesive model and the logarithmic extrapolation scheme is presented. The logarithmic extrapolation scheme is compared and validated against an empirical extrapolation scheme that is also developed, The logarithmic scheme is shown to be easier to implement in an implicit finite element code and more versatile. The schemes are used to capture high cycle fatigue growth accurately for a brittle Aluminium alloy and is shown to speed up simulations by a factor of two hundred.

The cohesive model is also used to predict overload simulations on 316L steel and the FEM simulations support FASEM based observations from experiments, which suggest that strain hardening and residual stresses, not crack closure, are the main causes of crack retardation seen in the overload effect.

Appendix A

Algorithm for solving damage evolution equations

The algorithm for solving the evolution equations for the damage variable κ is presented here. The incremental solution for the damage at each time step is obtained by the backward Euler method, using the value of κ from the previous time step and the derivative term as obtained from the evolution equations. Inputs to this algorithm are δ_n, δ_{n+1} and κ_n. Outputs are κ_{n+1} and T_{n+1}. Define $\dot{\delta}_{n+1} = \delta_{n+1} - \delta_n$.

If $\kappa_n > 1$

$\kappa_{n+1} = 1$

$T_{n+1} = 0$

return

end

If $\delta_n > \delta_u$

$\kappa_{n+1} = 1$

$T_{n+1} = 0.$

return

end

if $\dot{\delta}_{n+1} > 0$

$\alpha^* = \alpha$

else

$\alpha^* = -\gamma$

end

Solve the following system of four equations for κ_{n+1}, $\Delta\kappa_{n+1}$, T_{n+1}, C_{n+1}:

$\Delta\kappa_{n+1} = \alpha^*\kappa_{n+1}(T_{n+1} - \beta C_{n+1})(\Delta\delta_{n+1})$ (see (2.4))

$T_{n+1} = \frac{\sigma_c(1-\kappa_{n+1})\delta_{n+1}}{\kappa_{n+1}(\delta_u-\delta_c)+\delta_c}$ (see (2.1))

$C_{n+1} = \sigma_c(1 - \kappa_{n+1})$ (see (2.3))

$\kappa_{n+1} = \kappa_n + \Delta\kappa_{n+1}$ (backward Euler)

(Refer to the note below for the solution procedure.)

Let threshold = $\dot{\delta}_{n+1}(T_{n+1} - \beta C_{n+1})$

If $(threshold \cdot \dot{\delta}_{n+1}) > 0$

Execute OverStrengthCheck. (below)

return

else

$\kappa_{n+1} = \kappa_n$

$T_{n+1} = F(\kappa_n)\delta_{n+1}$

$C_{n+1} = C_n$

Execute OverStrengthCheck. (below)

return

end

The system of four equations described in this algorithm is solved using the following procedure. Observe that we can eliminate all the variables except κ_{n+1} using the obvious substitutions. After this elimination, the following cubic is obtained:

$$a\kappa_{n+1}^3 + b\kappa_{n+1}^2 + c\kappa_{n+1} + d = 0 \qquad \text{(A.1)}$$

where

$$\begin{aligned} a &= \beta\sigma_c\alpha^*\Delta\delta_{n+1}(\delta_u - \delta_c,) \\ b &= -[(\delta_{n+1} - \beta\delta_c)\sigma_c\alpha^*\Delta\delta_{n+1} + \beta\sigma_c\alpha^*\Delta\delta_{n+1}(\delta_u - \delta_c) + (\delta_u - \delta_c),] \\ c &= [\sigma_c\alpha^*\Delta\delta_{n+1}(\delta_{n+1} - \beta\delta_c) - \delta_c + \kappa_n(\delta_u - \delta_c),] \\ d &= \kappa_n\delta_c. \end{aligned}$$

Define a cubic function

$$\phi(\kappa) = a\kappa^3 + b\kappa^2 + c\kappa + d.$$

The cubic equation can be solved using the method of bisection. It is easy to see that $\phi(0) > 0$ and $\phi(1) < 0$. Therefore, there is at least one root of ϕ in $[0, 1]$. Furthermore, the number of roots is odd, i.e., either one or three of the cubic's roots are in this interval. In fact, for $|\alpha^*|$ sufficiently small, there is only one root. The reason is that for $|\alpha^*|$ sufficiently small,

$$\phi'(1) \approx (\kappa_n - 1)(\delta_u - \delta_c) - \delta_c < 0.$$

Since ϕ' is a convex quadratic, if $\phi'(1) < 0$ then ϕ' has at most one root in $[0, 1]$, which means that ϕ has at most one turning point in $[0, 1]$. This makes it impossible for ϕ to have three roots in the interval.

Procedure OverStrengthCheck

if $\dot{\delta} > 0$ and $T_{n+1} \geq C_{n+1}$

$\kappa_{n+1} = \frac{\delta_{n+1} - \delta_c}{\delta_f - \delta_c}$

$T_{n+1} = F(\kappa_{n+1})\delta_{n+1}$

end

BIBLIOGRAPHY

[1] Standard test method for measurement of fatigue crack growth rates. *ASTM*, 2000. E 647-99.

[2] *ABAQUS,INC.*, 2005. ABAQUS/standard users manual, version 6.5.

[3] T.L. Anderson. *Fracture Mechanics: Fundamentals and Applications*. CRC Press, 1995.

[4] A. de Andres, J. L. Perez, and M. Ortiz. Elastoplastic finite element analysis of three-dimensional fatigue crack growth in aluminum shafts subjected to axial loading. *IJSS*, 36:2231–2258, 1999.

[5] W. Elber. The significance of fatigue crack closure. *American Society for Testing and Materials*, 486:230–242, 1971.

[6] X.Z. Hu Y. Estrin G. Wheatley, R.Niefanger. Fatigue crack growth in 316l stainless steel. *Key Engineering Materials*, 145-149:631–636, 1998.

[7] Y. Estrin G. Wheatley, X.Z. Hu. Effects of a single tensile overload on fatigue crack growth in a 316l steel. *Fatigue and Fracture of Engineering Materials and Structures*, 22(12):10411051, 1999.

[8] S. Maiti and P.H. Geubelle. A cohesive model for fatigue failure of polymers. *Engineering Fracture Mechanics*, 72(36):691–708, 2005.

[9] O. Nguyen, E. A. Repetto, M. Ortiz, and R. A. Radovitzky. A cohesive model of fatigue crack growth. *IJF*, 110:351–369, 2001.

[10] M. Ortiz and A. Pandolfi. Finite-deformation irreversible cohesive elements for three dimensional crack propagation analysis. *IJNME*, 44:1267–1282, 1999.

[11] K. D. Papoulia, S. A. Vavasis, and P. Ganguly. Spatial convergence of crack nucleation using a cohesive finite element model on a pinwheel-based mesh. *IJNME*, 67(1):1–16, 2006.

[12] P. C. Paris and F. Erdogan. A critical analysis of crack propagation. *Trans. ASME. J Basic Eng.*, 85:528–534, 1963.

[13] P. C. Paris, M. P. Gomez, and W. E. Anderson. A rational theory of fatigue. *The Trend in Eng.*, 13:9–14, 1961.

[14] K. L. Roe and Siegmund T. An irreversible cohesive zone model for interface fatigue crack growth simulation. *Engineering Fracture Mechanics*, 70:209–232, 2001.

[15] R. I. Stephens, H. D. Berns, R. A. Chernenkoff, R. L. Indig, S. K. Koh, D. J. Lingenfelser, M. R. Mitchell, R. A. Testin, and W. W. Wigant. *Fatigue and Fracture Toughness of A356-T6 Cast Aluminum Alloy, society of automotive engineers, Inc., Pensylvania*, 1988.

[16] S. Suresh. *Fatigue of Materials*. Cambridge University Press, 1998.

[17] A. Ural, V.R. Krishnan, and K. D. Papoulia. Cohesive fracture model for fatigue allowing for crack closure. *IJSS, in revision*, 2008.

[18] A. Ural and K. D. Papoulia. Modeling of fatigue crack growth with a damage-based cohesive zone model. In *Proceedings, European Congress on Computational Methods in Applied Sciences and Engineering ECCOMAS 2004, P. Neittaanmaki et al. (eds)*, Jyvaskyla, Finland, 2004.

[19] Ani Ural. *Damage based cohesive model for predicting fatigue crack growth*. PhD thesis, Cornell University, 2005.

[20] X.-P. Xu and A. Needleman. Numerical simulations of fast crack growth in brittle solids. *JMPS*, 42:1397–1434, 1994.